Synthesis, physicochemical characterization and antiproliferative activity of phosphino Ru(II) and Ir(III) complexes.

Urszula K. Komarnicka,[a†]* Sandra Kozieł,[a†] Agnieszka Skórska-Stania,[b] Agnieszka Kyzioł,[b] Francesco Tisato[c]

[a.] *Faculty of Chemistry, University of Wroclaw, Joliot-Curie 14, 50-383 Wroclaw, Poland*

[b.] *Faculty of Chemistry, Jagiellonian University in Krakow, Gronostajowa 2, 30-387 Krakow, Poland*

[c.] *ICMATECNR, Corso Stati Uniti4, 35127 Padova, Italy*

[†] *First Author, *corresponding Author: urszula.komarnicka@chem.uni.wroc.pl*

Herein we present the synthesis of new complexes based on ruthenium(II) (Ru(η^6-*p*-cymene)$Cl_2PPh_2CH_2OH$ (RuPOH), Ru(η^6-p-cymene)$Cl_2P(p\text{-}OCH_3Ph)_2CH_2OH$ (RuMPOH)) and iridium(III) (Ir(η^5-Cp*)$Cl_2P(p\text{-}OCH_3Ph)_2CH_2OH$ (IrMPOH), Ir(η^5-Cp*)$Cl_2PPh_2CH_2OH$ (IrPOH) containing phosphine ligands with/without methoxy motif on phenyl rings ($P(p\text{-}OCH_3Ph)_2CH_2OH$ (MPOH) and PPh_2CH_2OH (POH)). The complexes were characterized by mass spectrometry, NMR spectroscopy (1D: ^1H, $^{13}C\{^1H\}$, $^{31}P\{^1H\}$, 2D: HMQC, HMBC, COSY NMR) and elemental analysis. All the complexes were structurally identified by single-crystal X-ray diffraction analysis. The Ru(II) and Ir(III) complexes have typical piano-stool geometry with a η^6-coordinated arene (Ru^{II}complexes) or η^5-coordinated (Ir^{III} compunds) and three additional sites of ligation occupied by two chloride ligands and the phosphine ligand. Oxidation of NADH to NAD^+ with high efficiency was catalyzed by complexes containing $P(p\text{-}OCH_3Ph)_2CH_2OH$ (IrMPOH and RuMPOH). The catalytic property might have important future applications in biological and medical fields like production of reactive oxygen species (ROS). Furthermore redox activity of complexes was confirmed by cyclic voltamperometry. Biochemical assays demonstrated the ability of Ir(III) and Ru(II) complexes to induce significant cytotoxicity in various cancerous cell lines. Furthermore we found that RuPOH and RuMPOH selectively inhibit proliferation of skin cancer cells (WM266-4; IC_{50}, after 24h: *av.*48.3 μM; after 72h: *av.*10.2 μM) while Ir(III) complexes were found to be moderately active against prostate cancer cells (DU145).

Graphical Abstract

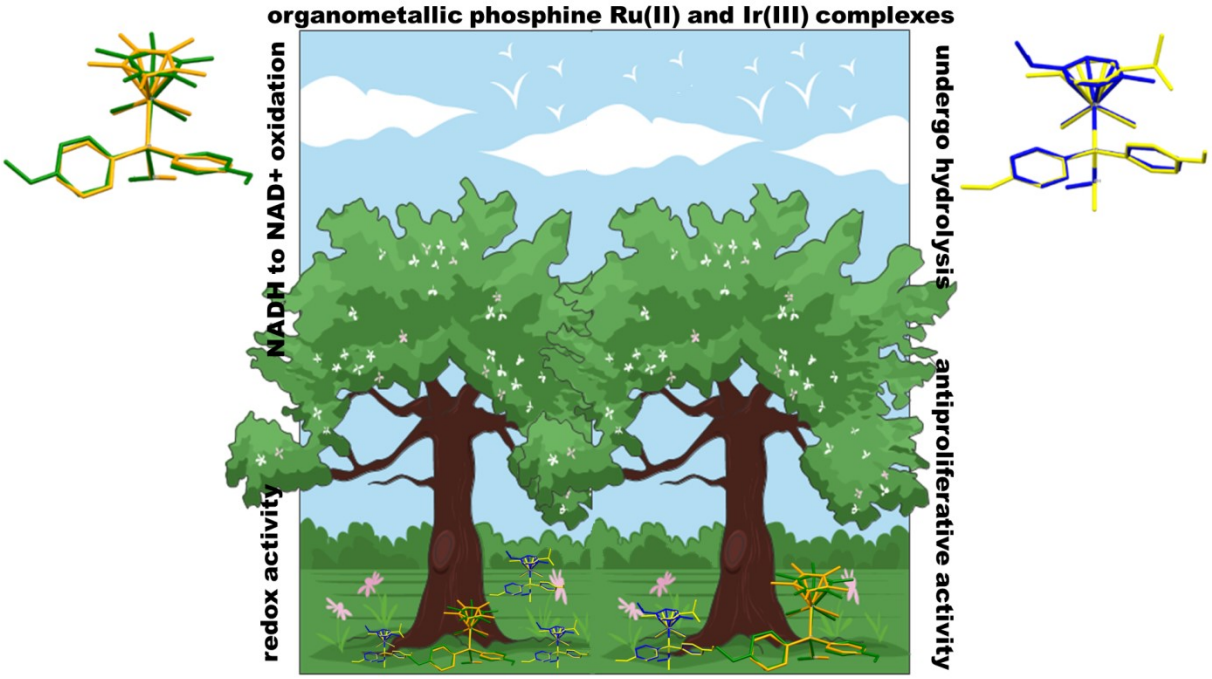

Table S1. Crystallographic experimental details.

Identification code	**RuPOH**	**IrPOH**	**RuMPOH**	**IrMPOH**
Crystal data				
Empirical formula	C23H27Cl2OPRu	C23H28Cl2IrOP	C25H31Cl2O3PRu	C25H32Cl2IrO3P
Formula weight	522.38	614.52	582.44	674.57
Temperature [K]	100(2)	293(2)	293(2)	100(2)
Wavelength [Å]	1.54184	0.71073	0.71073	1.54184
Crystal system, space group	Monoclinic, P 2_1	Monoclinic, P $2_1/n$	Monoclinic, P $2_1/n$	Monoclinic, P $2_1/n$
a, b, c [Å]	7.6065(1), 13.8332(1), 10.7154(1)	10.5605(1), 17.1832(2), 12.7618(1)	9.6600(1), 11.1867(1), 23.5077(3)	8.5562(2), 20.6545(6), 13.9418(2)
β [°]	105.490(1)	93.613(1	92.598(1)	92.251(2)
V [Å^3]	1086.54(2)	2311.19(4)	2537.71(5)	2461.95(10)
Z	2	4	4	4
Radiation type	Cu K_α	Mo K_α	Mo K_α	Cu K_α
μ [mm^{-1}]	8.881	6.089	0.916	13.313
Crystal size [mm]	0.40 x 0.25 x 0.10	0.20 x 0.20 x 0.20	0.50 x 0.30 x 0.20	0.10 x 0.05x 0.01
Data collection				
Diffractometer	Rigaku (Cu) XtaLAB Synergy-DW VHF with a HyPix-Arc 150 detector	Rigaku OD SuperNova Dual source with an Atlas detector	Rigaku OD SuperNova Dual source with an Atlas detector	Rigaku (Cu) XtaLAB Synergy-DW VHF with a HyPix-Arc 150 detector
Absorption correction	Multi-scan (*CrysAlisPRO*; Rigaku OD, 2020)	Multi-scan (*CrysAlis PRO*; Rigaku OD, 2015)	Multi-scan (*CrysAlis PRO*; Rigaku OD, 2015)	Multi-scan (*CrysAlisPRO*; Rigaku OD, 2020)
No. of measured, independent and observed [I > 2σ(I)] reflections	9002/8981/3776	35098/6202/5185	37574/6823/5422	27876/5031/4572
R(int)	0.0360	0.0397	0.0388	0.0482
Completeness	99.7 %	99.6 %	99.8 %	99.6 %
Refinement				
Data / restraints / parameters	9002 / 1 / 261	6201 / 0 / 270	6823 / 0 / 297	5031 / 0 / 297
R[F2 > 2σ(F2)], wR(F2), S	0.0191, 0.0497, 1.201	0.0220, 0.0411, 1.075	0.0305, 0.0626, 1.069	0.0394, 0.1008, 1.095
Δρmax, Δρmin (e Å-3)	0.376 and -0.427	0.850 and -0.614	0.350 and -0.470	1.426 and -2.097

Rigaku OD (2015). CrysAlis PRO. Rigaku Oxford Diffraction Ltd, Yarnton, Oxfordshire, England.

Rigaku OD (2020). *CrysAlis PRO*. Rigaku Oxford Diffraction, Yarnton, England.

Sheldrick, G. M. (2015*a*). *Acta Cryst.* A**71**, 3–8

Table S2. Hydrogen-bond geometry (Å, °)

D-H...A	d(D-H)	d(H...A)	d(D...A)	<(DHA)
RuPOH				
C11-H11A...Cl2	0.99	2.89	3.487(4)	120.0
O11-H11...Cl1	0.80(6)	2.30(6)	3.059(3)	159(5)
IrPOH				
C26-H26...Cl1	0.93	2.87	3.640(3)	140.5
C32-H32...Cl2	0.93	2.96	3.606(3)	127.6
O11B_a-H1OB_a...Cl1	0.82	2.20	2.957(3)	153.0
O11A_b-H1OA_b...Cl2	0.82	2.32	3.099(9)	159.7
RuMPOH				
C11-H11A...Cl1	0.97	2.76	3.336(2)	118.6
C11-H11B...Cl2	0.97	2.78	3.355(2)	118.4
C25-H25...O34_#1	0.93	2.47	3.313(3)	150.8
C27-H27C...Cl2_#2	0.96	2.97	3.870(3)	157.5
C33-H33...Cl2_#3	0.93	2.83	3.426(2)	122.6
O11-H11O...Cl1_#2	0.77(3)	2.50(3)	3.259(2)	171(3)
Symmetry transformations used to generate equivalent atoms:				
#1 -x-1/2, y+1/2, -z+3/2 #2 -x, -y, -z+1 #3 -x+1/2, y+1/2, -z+3/2				
IrMPOH				
C23-H23...Cl1#1	0.95	2.72	3.444(6)	133.5
C32-H32...Cl1	0.95	2.84	3.667(6)	145.4
C33-H33...Cl2#2	0.95	2.99	3.590(6)	122.6
O11-H11...Cl2	0.84	2.39	3.186(5)	157.2
Symmetry transformations used to generate equivalent atoms:				
#1 x-1/2,-y+1/2,z+1/2 #2 x-1/2,-y+1/2,z-1/2				

Table S3. Cumulative NMR data (298 K, δ [ppm], J [Hz]) for ligands (in $CDCl_3$) and iridium-complexes (in CD_2Cl_2).

	POHC[40]	**MPOHC**[42]	**POH**[41]	**MPOH**[42]	**[Ir(η⁵-Cp*)Cl₂]₂**[a]	**[Ru(η⁶-p-cymene)Cl₂]₂**	**IrPOH**	**IrMPOH**	**RuPOH**	**RuMPOH**
^{31}P	**-11.46**	**15.23**	**-9.33**	**-13.60**			**-7.15**	**-9.18**	**16.74**	**15.07**
$H^{Ph(m)}$	7.52-7.21	7.25-7.82	7.60-7.31	7.25-7.82			7.41-7.54 m	7.70 t (9.34)	7.41-7.58 m	7.77 t (9.07)
$H^{Ph(o)}$							7.72-7.84 m	6.98 dd (8.80; 1.50)	7.79-7.93 m	6.98 dd (8.66; 1.40)
H^{1}	4.32 d (7.7)	5.03 s	4.42 d (8.39)	4.27 d (9.01)			4.97 d (6.6)	4.86 s	4.64 s	4.54 s
H^{-OH}		not observed	1.80 m	not observed			not observed	not observed	not observed	not observed
H^{-OCH3}		3.87 s		3.74 s				3.85 s		3.86 s
$C^{Ph(i)}$	135.65 d (12.0)	106.89 d (84.47)	135.65 d (12.0)	126.28 d (9.08)				118.82 d (55.4)	132.49 d (15.2)	123.14 d (47.23)
$C^{Ph(o)}$	132.91 d (17.6)	115.63 d (7.54)	132.91 d (17.6)	114.41 d (7.27)			133.80 d (9.9)	113.93 d (10.9)	133.61 d (9.1)	114.15 s
$C^{Ph(m)}$	128.39 d (5.6)	135.61 d (9.99)	128.39 d (5.6)	134.58 d (19.07)			128.15 d (9.9)	135.57 d (10.9)	128.55 d (9.1)	135.02 s
$C^{Ph(p)}$	128.64 s	164.03 s	128.64 s	160.42 s			130.92 s	161.83 s	131.17 s	161.68 s
C^{1}	62.46 d (13.0)	53.31 d (59.04)	62.46 d (13.0)	62.94 d (14.53)			64.25 d (39.1)	64.87 d (31.06)	63.28 d (40.1)	63.51 d (31.79)
C^{-OCH3}		55.86 s		55.23 s				55.35 s		55.39 s
$H^{Cp*(CH3)}$					0.96 s		1.40 d (2.19)	1.40 d (2.19)		
$H^{2,3}$						1.29 d (6.9)			0.93 d (7.0)	0.97 d (6.98)
H^{4}						2.93 spt (7.0)			2.56 spt (7.0)	2.61 spt (7.00)
$H^{6,7,8,9}$						5.42 dd (19.2; 6.0)			5.27 dd (19.6; 6.2)	5.25 s
H^{11}						2.16 s			1.91 s	1.89 s
$C^{Cp*(CH3)}$					9.38 s		8.08 s	8.35 s		
C^{Cp*}					86.28 s		92.28 d (2.2)	92.34 d (2.72)		
$C^{2,3}$						22.12 s			21.73 s	21.60 s
C^{4}						30.63 s			30.34 s	30.18 s
C^{5}						101.22 s			108.84 s	108.76 s
$C^{6,8}$						80.54 s			86.42 d (5.4)	86.19 s
$C^{7,9}$						81.32 s			89.74 d (3.6)	89.31 s
C^{10}						96.75 s			95.60 s	95.14 s
C^{11}						18.89 s			17.70 s	17.57 s

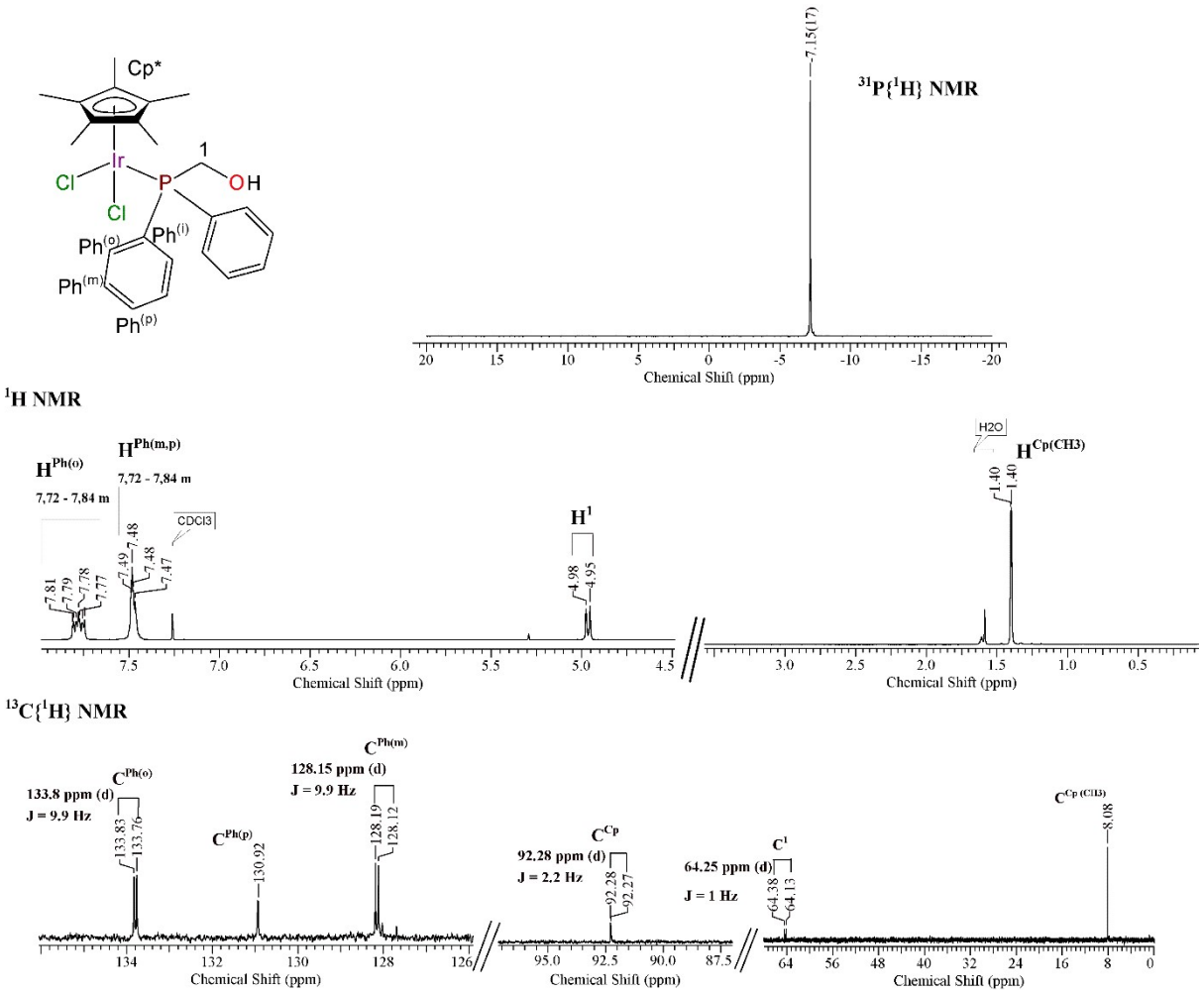

Figure S1. ^{1}H, $^{13}C\{^{1}H\}$ and $^{31}P\{^{1}H\}$ NMR spectra for **IrPOH** (298 K, $CDCl_3$).

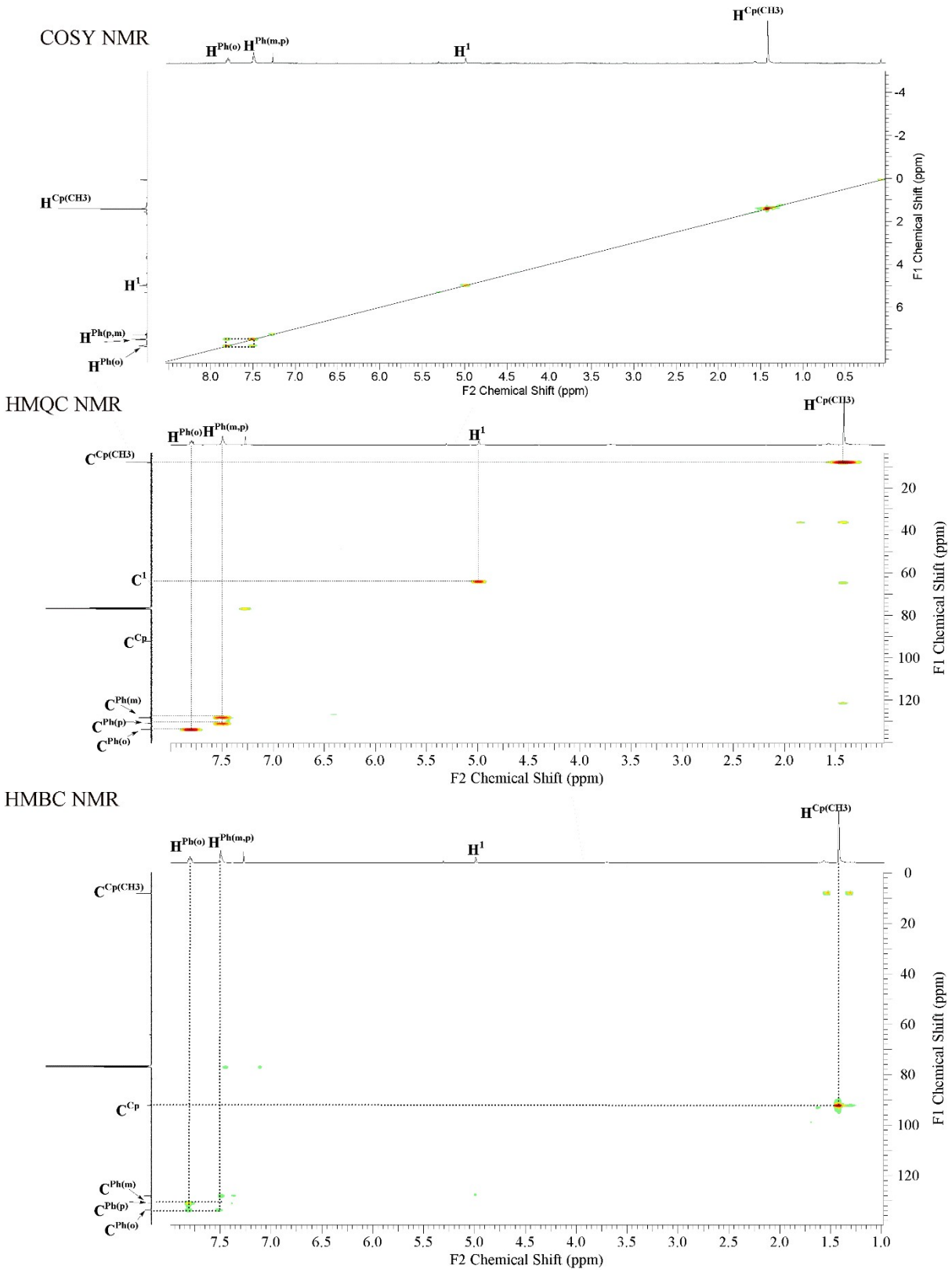

Figure S2. HMQC, HMBC, COSY NMR spectra for **IrPOH** (298 K, $CDCl_3$).

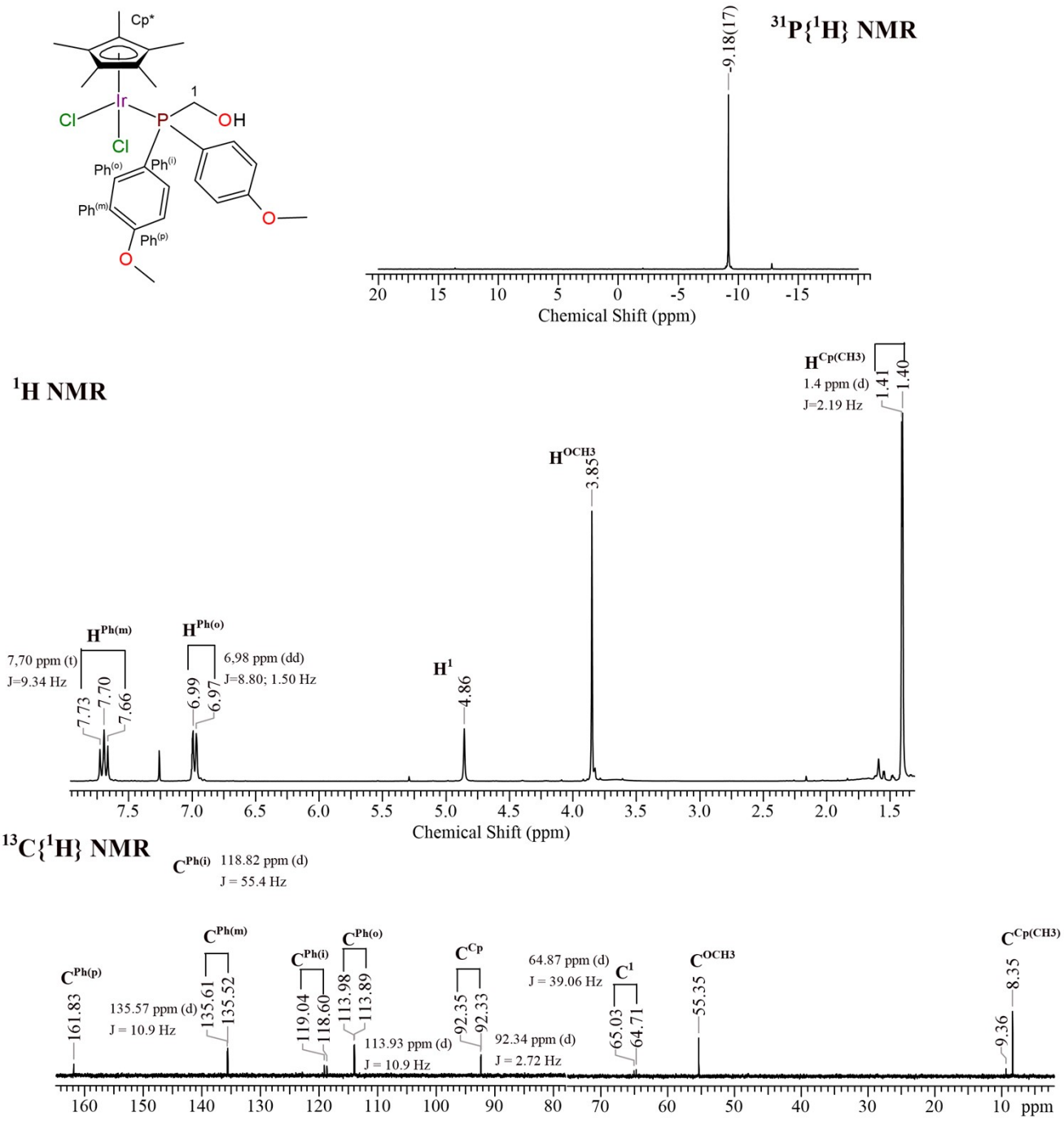

Figure S3. ^{1}H, $^{13}C\{^{1}H\}$ and $^{31}P\{^{1}H\}$ NMR spectra for **IrMPOH** (298 K, $CDCl_3$).

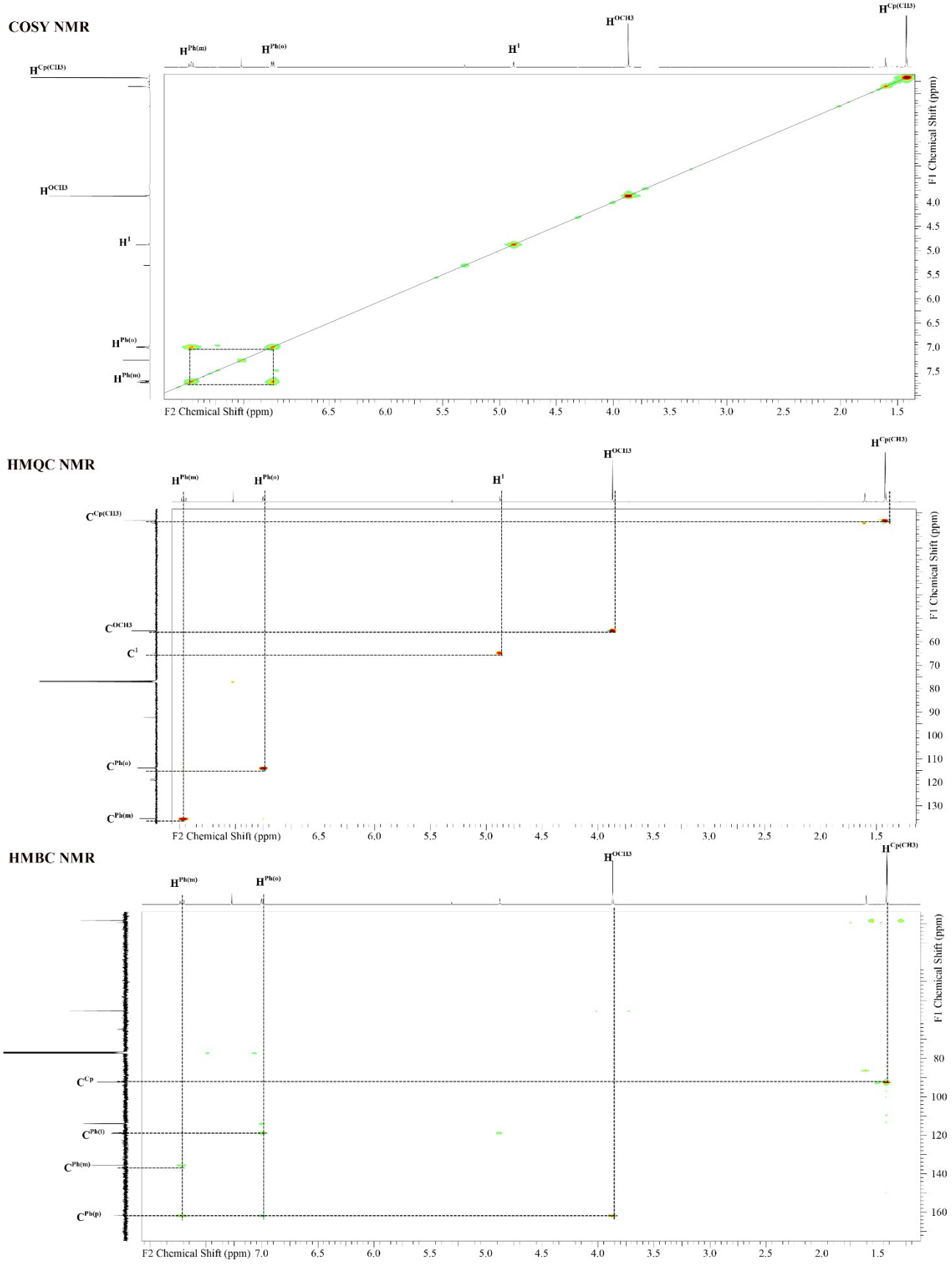

Figure S4. HMQC, HMBC, COSY NMR spectra for **IrMPOH** (298 K, $CDCl_3$).

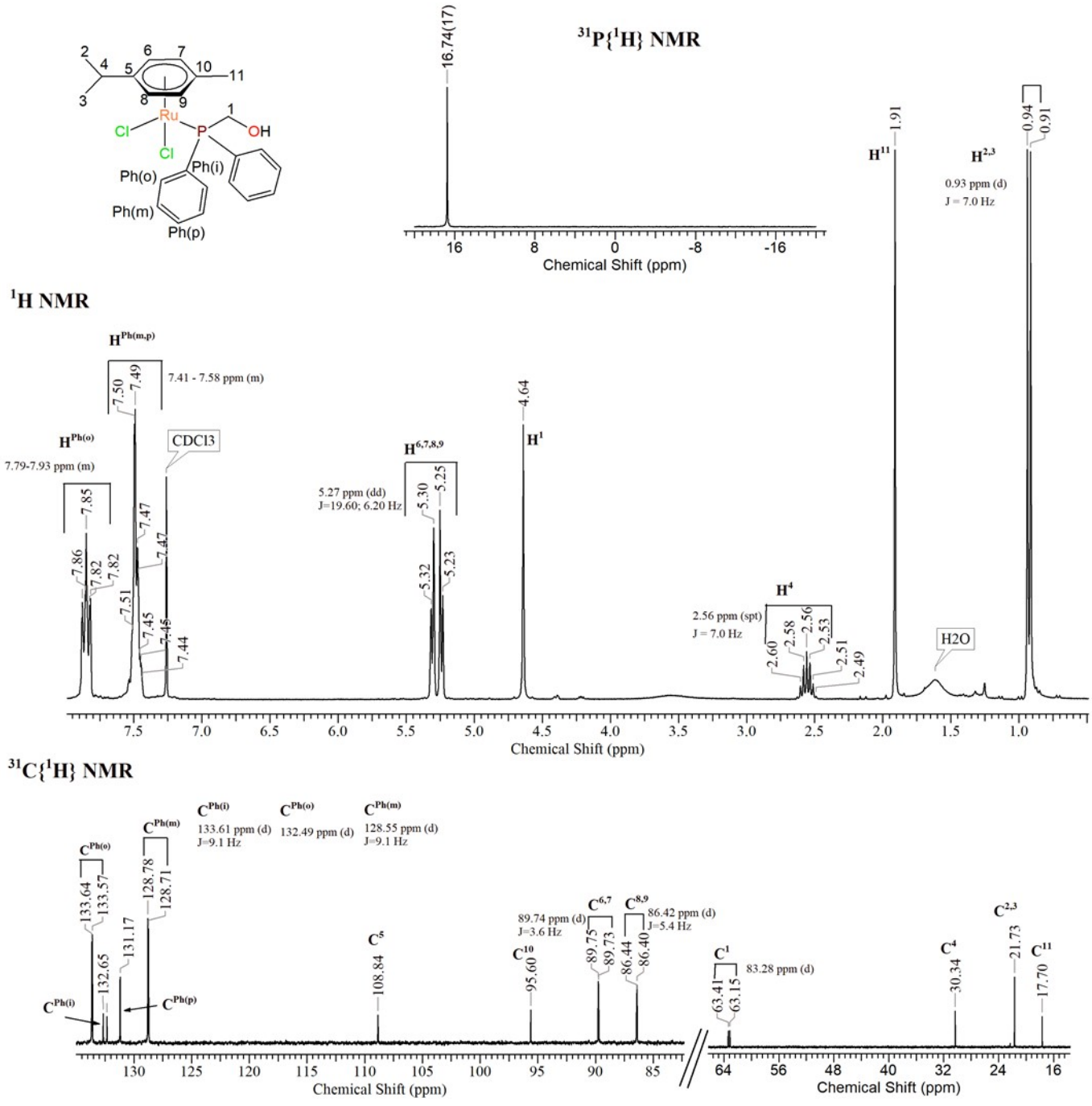

Figure S5. ^{1}H, $^{13}C\{^{1}H\}$ and $^{31}P\{^{1}H\}$ NMR spectra for **RuPOH** (298 K, $CDCl_3$).

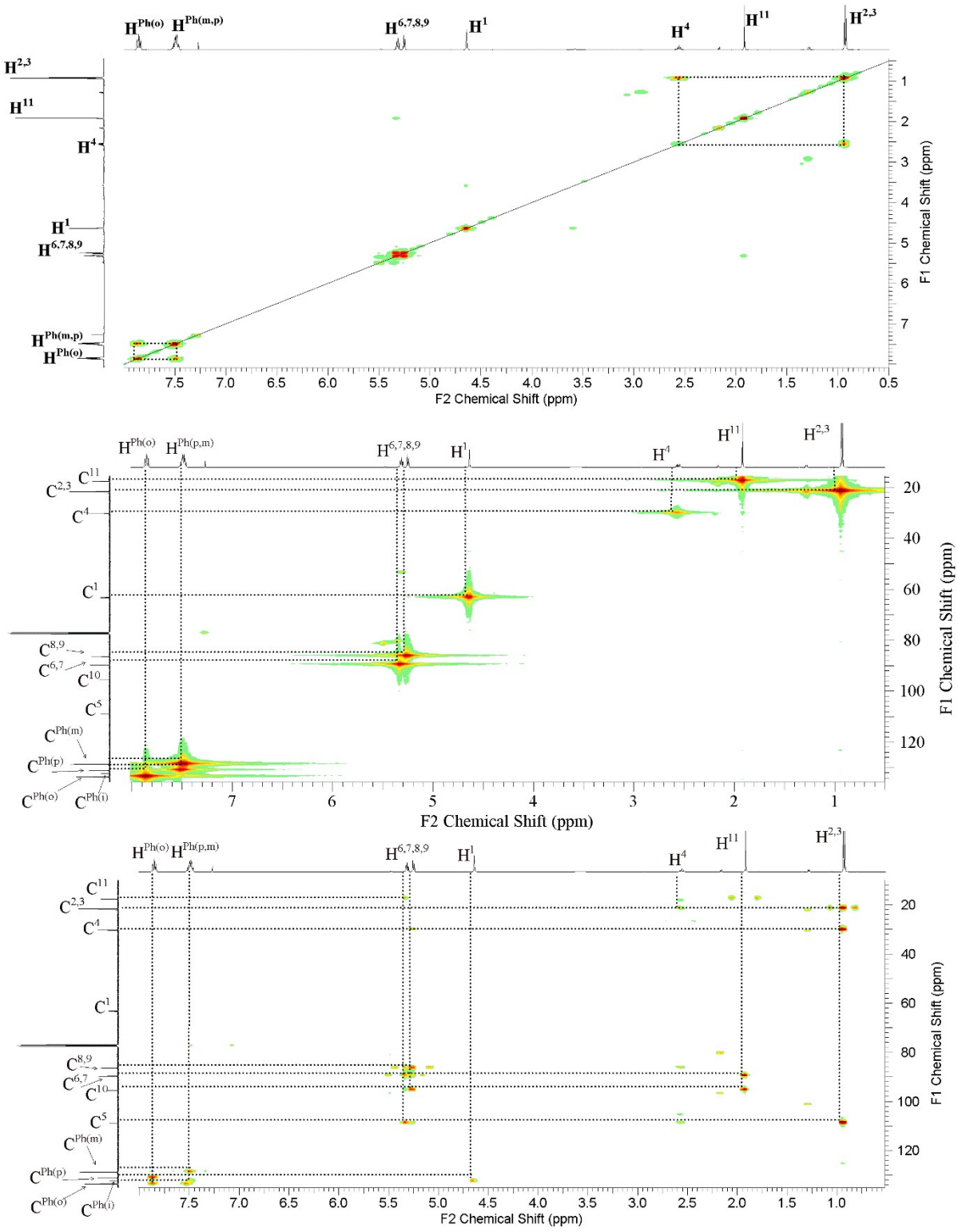

Figure S6. HMQC, HMBC, COSY NMR spectra for **RuPOH** (298 K, $CDCl_3$).

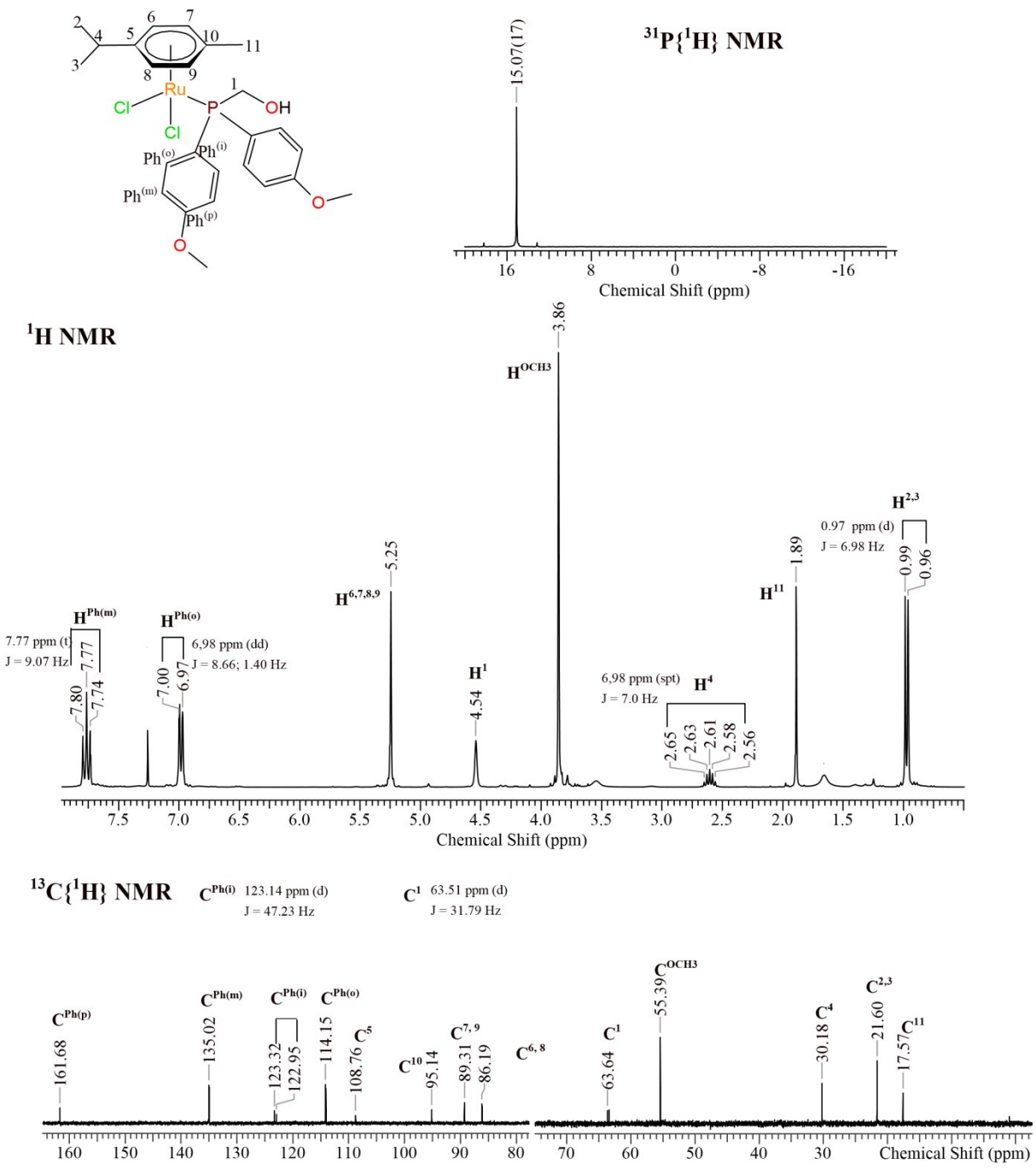

Figure S7. ^{1}H, $^{13}C\{^{1}H\}$ and $^{31}P\{^{1}H\}$ NMR spectra for **RuMPOH** (298 K, $CDCl_3$).

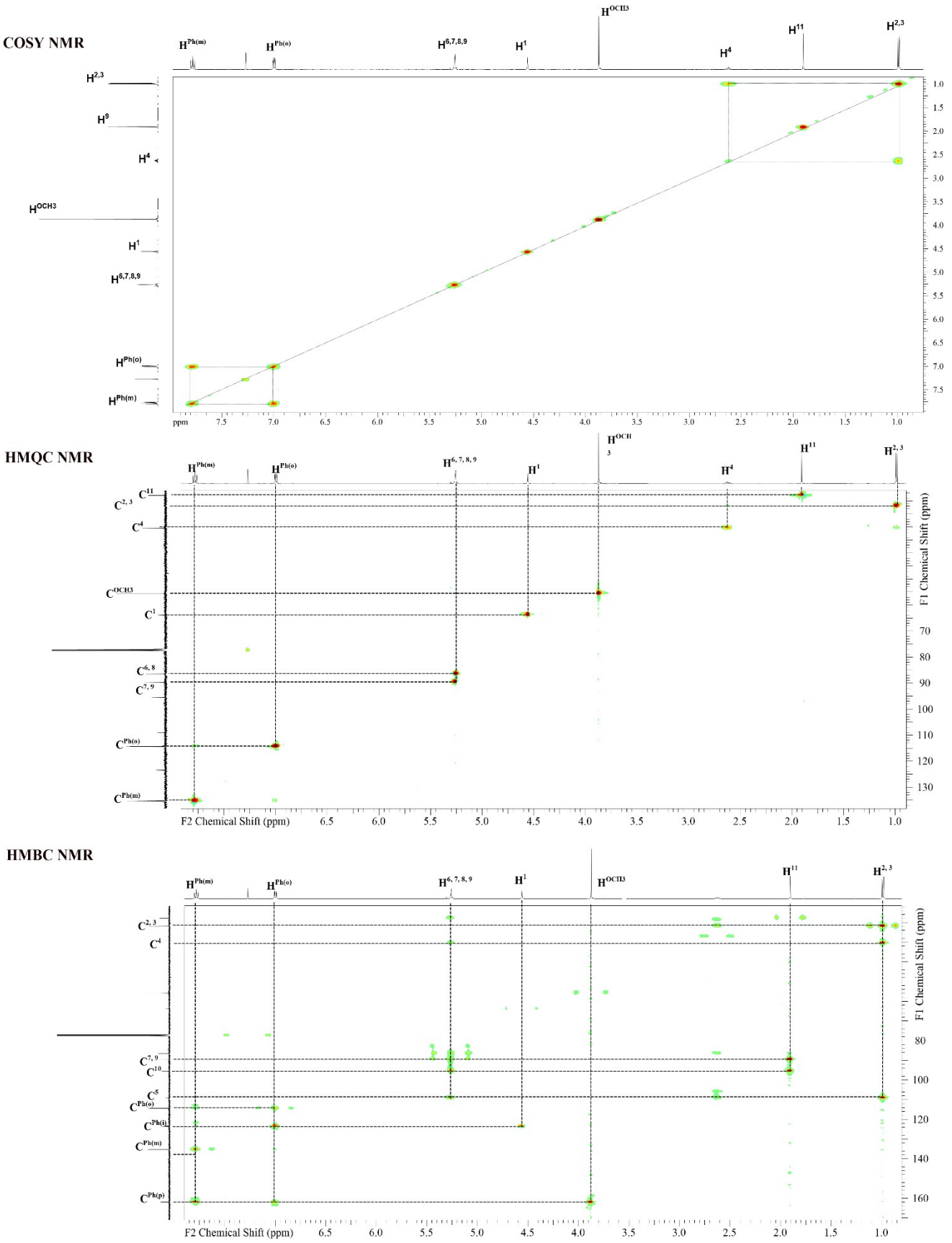

Figure S8. HMQC, HMBC, COSY NMR spectra for **RuMPOH** (298 K, $CDCl_3$).

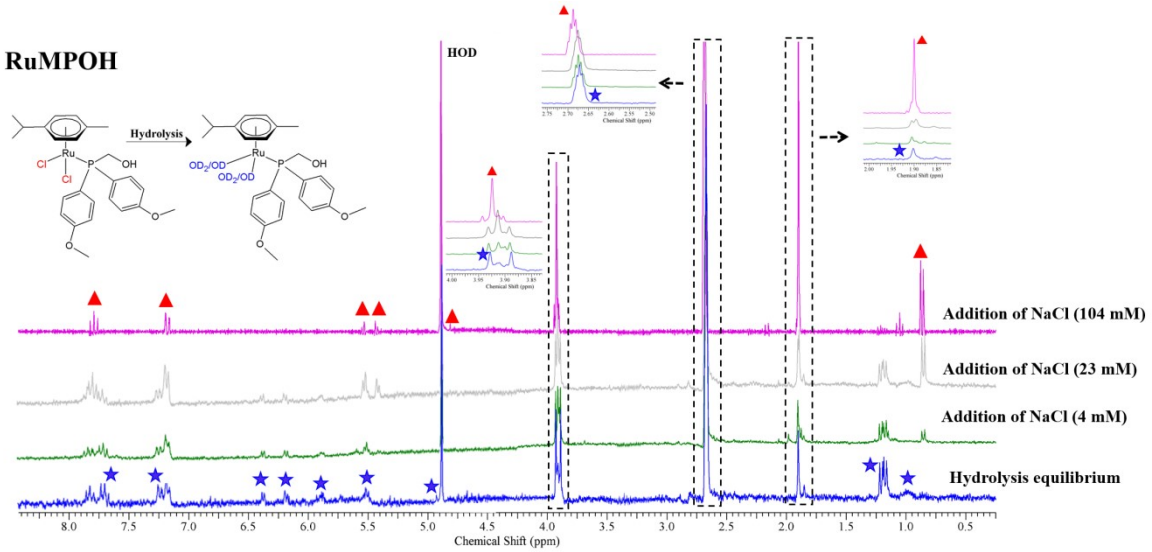

Figure S9. Confirmation of hydrolysis of **RuMPOH** by ^{1}H NMR in 20% DMSO-d_6/80% D_2O (v/v) at 298 K. From bottom to top: ^{1}H NMR spectrum of an equilibrium solution of **RuMPOH** (1 mM); spectrum recorded 10 min after addition of NaCl (final concentration, 4 mM) to the equilibrium solution of **RuMPOH**; final concentration of NaCl, 23mM; final concentration of NaCl, 104mM – respectivelyThe peaks for the chlorido complex **RuMPOH** (red triangle) increased in intensity while peaks for the aqua complex decreased (blue star).

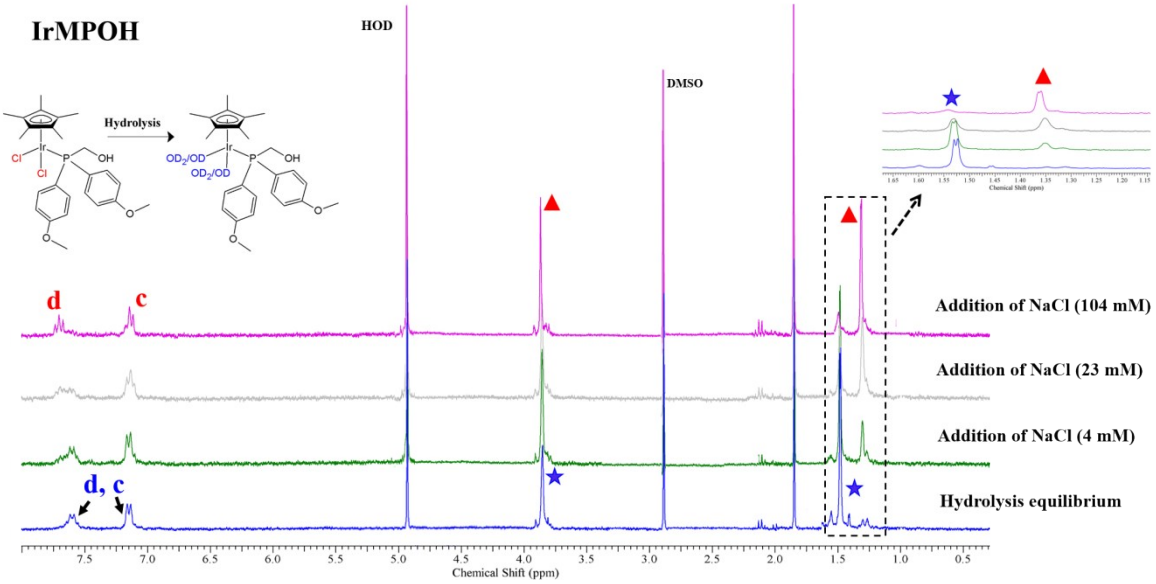

Figure S10. Confirmation of hydrolysis of **IrMPOH** by ^{1}H NMR in 20% DMSO-d_6/80% D_2O (v/v) at 298 K. From bottom to top: ^{1}H NMR spectrum of an equilibrium solution of **IrMPOH** (1 mM); spectrum recorded 10 min after addition of NaCl (final concentration, 4 mM) to the equilibrium solution of **IrMPOH**; final concentration of NaCl, 23mM; final concentration of NaCl, 104mM – respectively. The peaks for the chlorido complex **IrMPOH** (red triangle) increased in intensity while peaks for the aqua complex decreased (blue star).

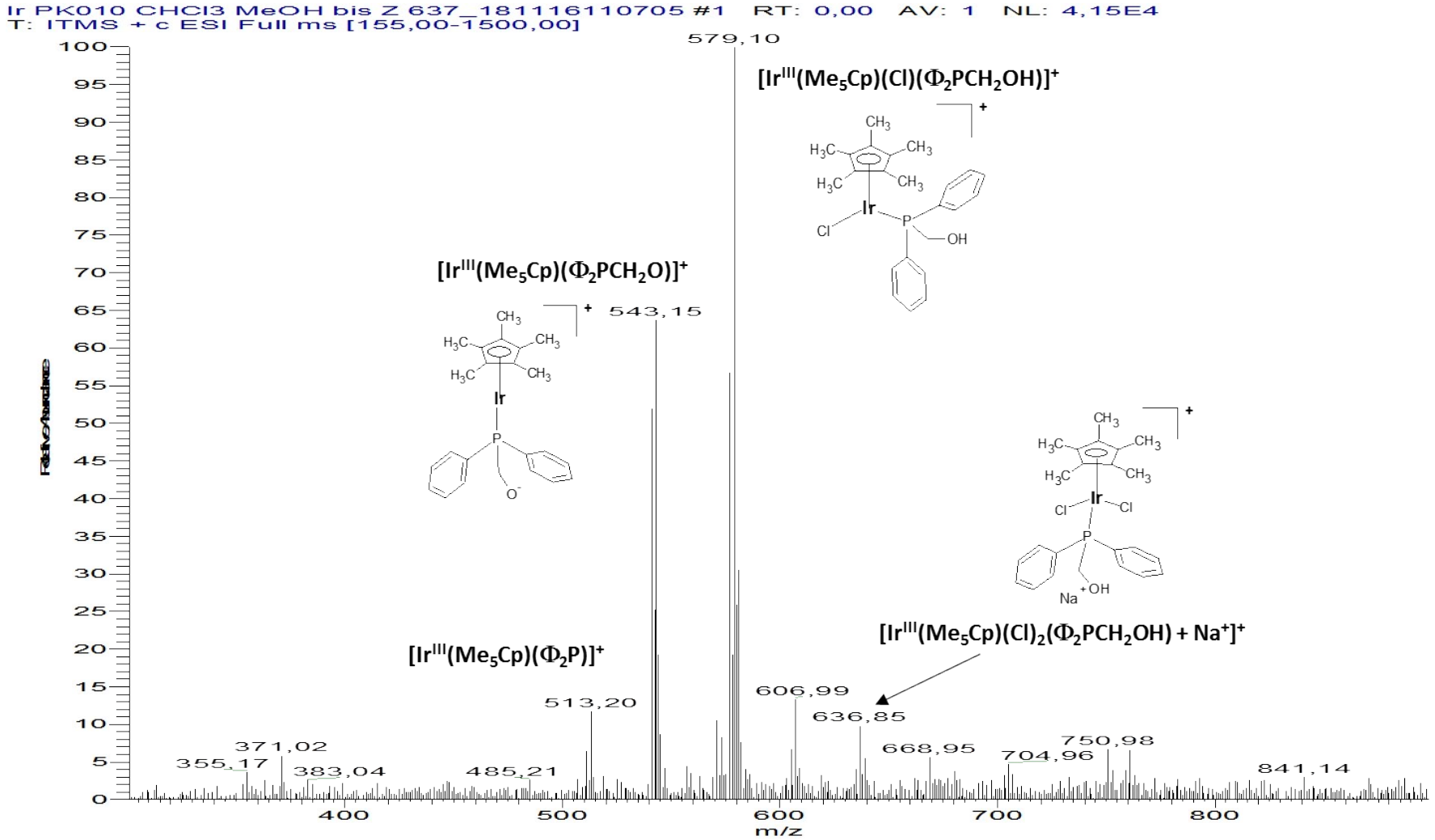

Figure S11. Full ESI(+)MS spectrum of **IrPOH**

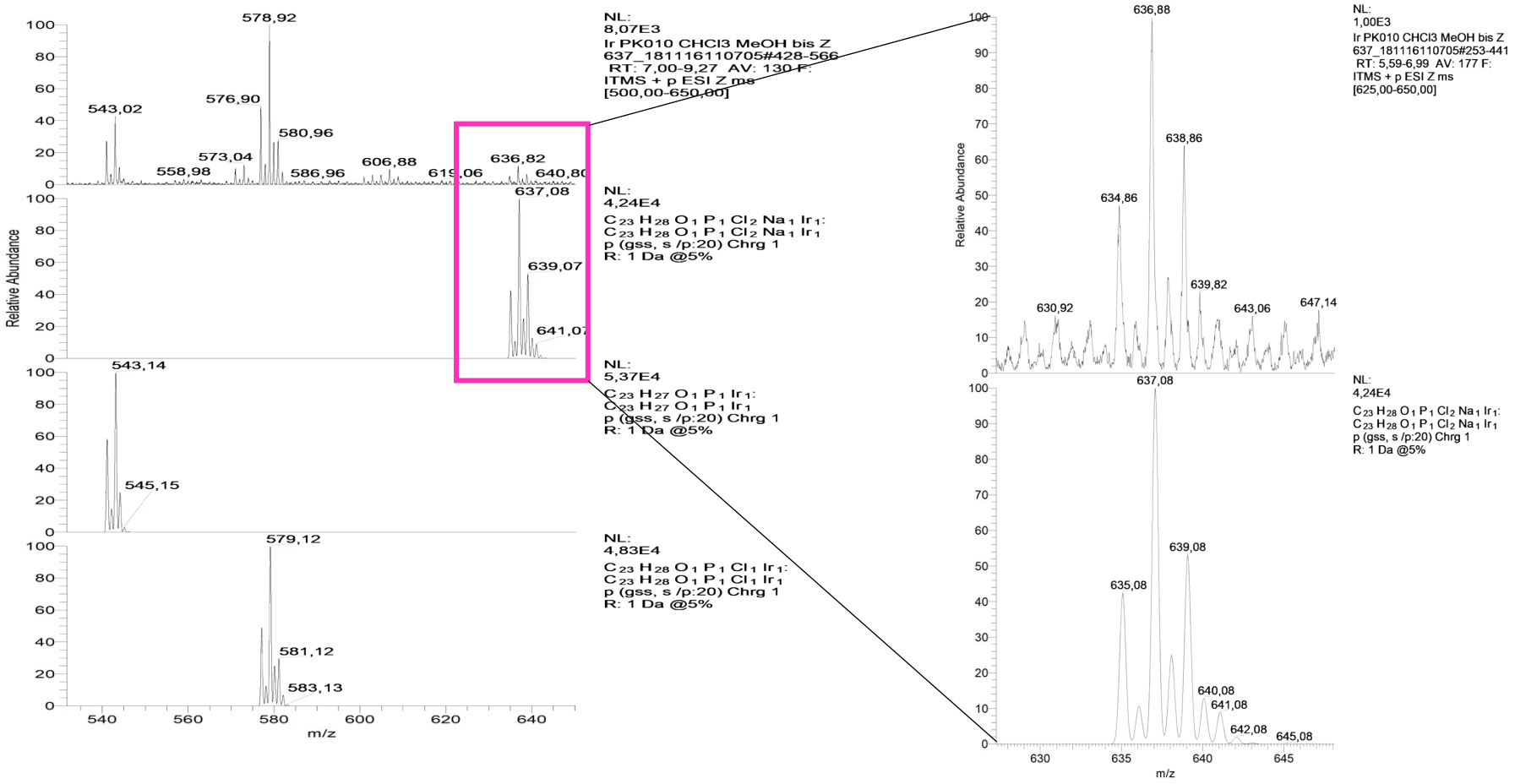

Figure S12. Comparison of ion peaks (experimental (top traces) vs calculated (bottom traces)) in the 630 – 650 m/z region of **IrPOH**. Note the different profile of the cluster centred at m/z 637 ($[Ir(Me_5\text{-}Cp)(Cl)_2(Ph_2PCH_2OH) + Na]^+$, containing the $IrCl_2$ moiety) with respect to that centered at m/z 579 ($[Ir(Me_5\text{-}Cp)(Cl)(Ph_2PCH_2OH)]^+$, containing the IrCl moiety), and to that centered at m/z 543 ($[Ir(Me_5\text{-}Cp)(Ph_2PCH_2O)]^+$, containing the Ir ion only).

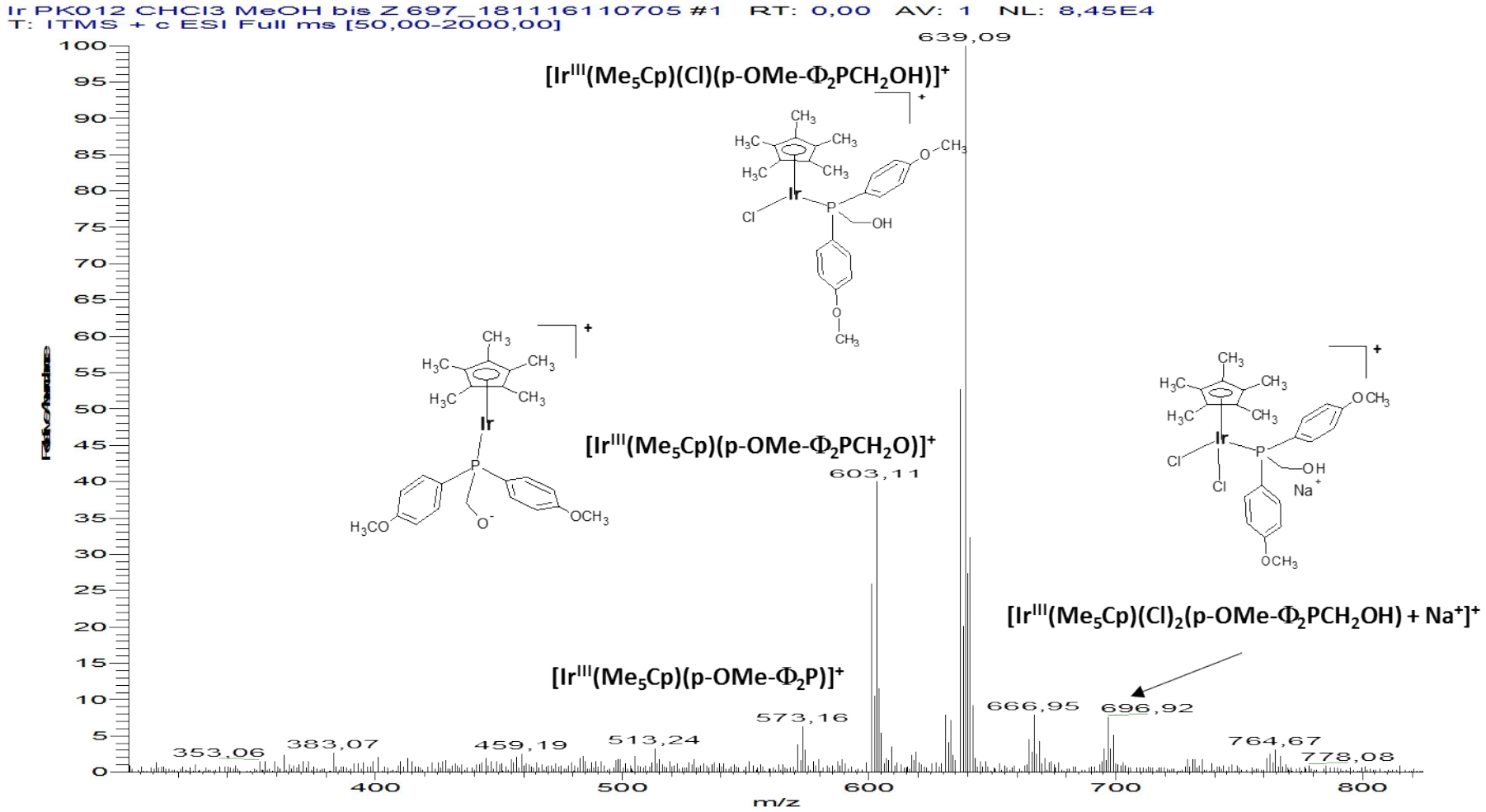

Figure S13. Full ESI(+)MS spectrum of **IrMPOH**.

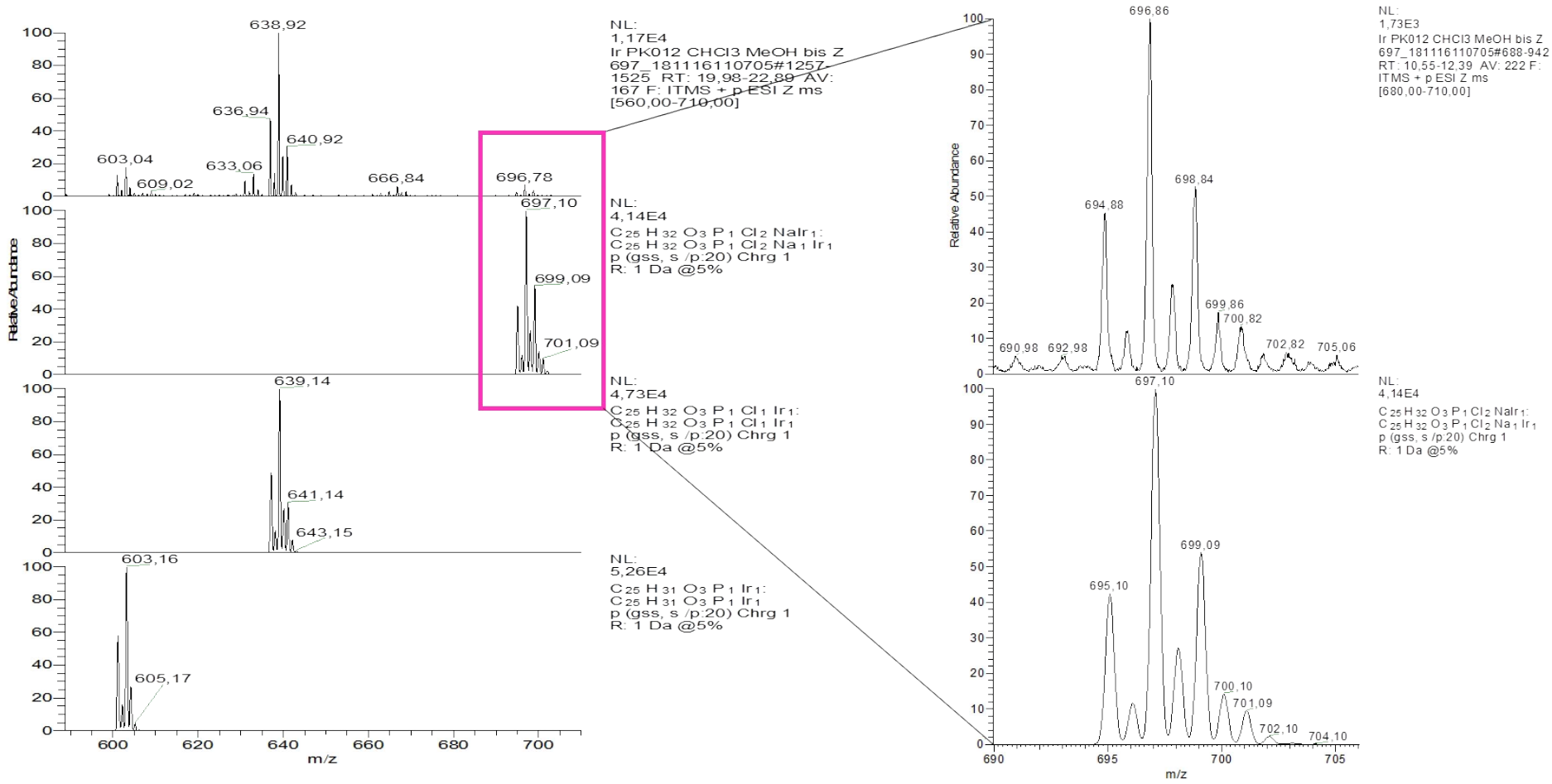

Figure S14 Comparison of high abundant cluster ion peaks (experimental vs calculated) in the 690 – 710 m/z region of **IrMPOH**. Note the different profile of the cluster centered at m/z 639 (containing the IrCl moiety) with respect to the other two profiles centered at m/z 603 and 573 (containing Ir only).

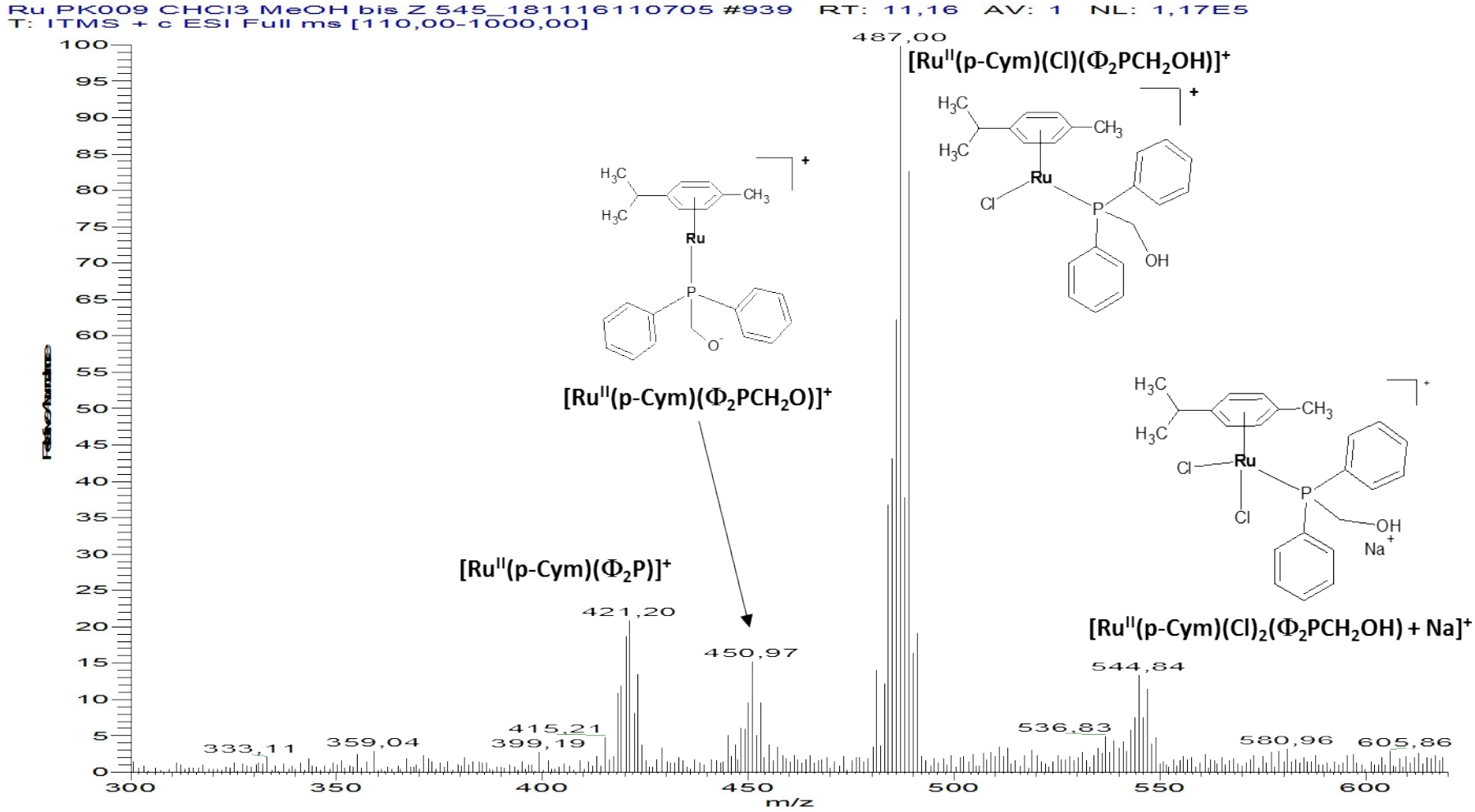

Figure S15. Full ESI(+)MS spectrum of **RuPOH**.

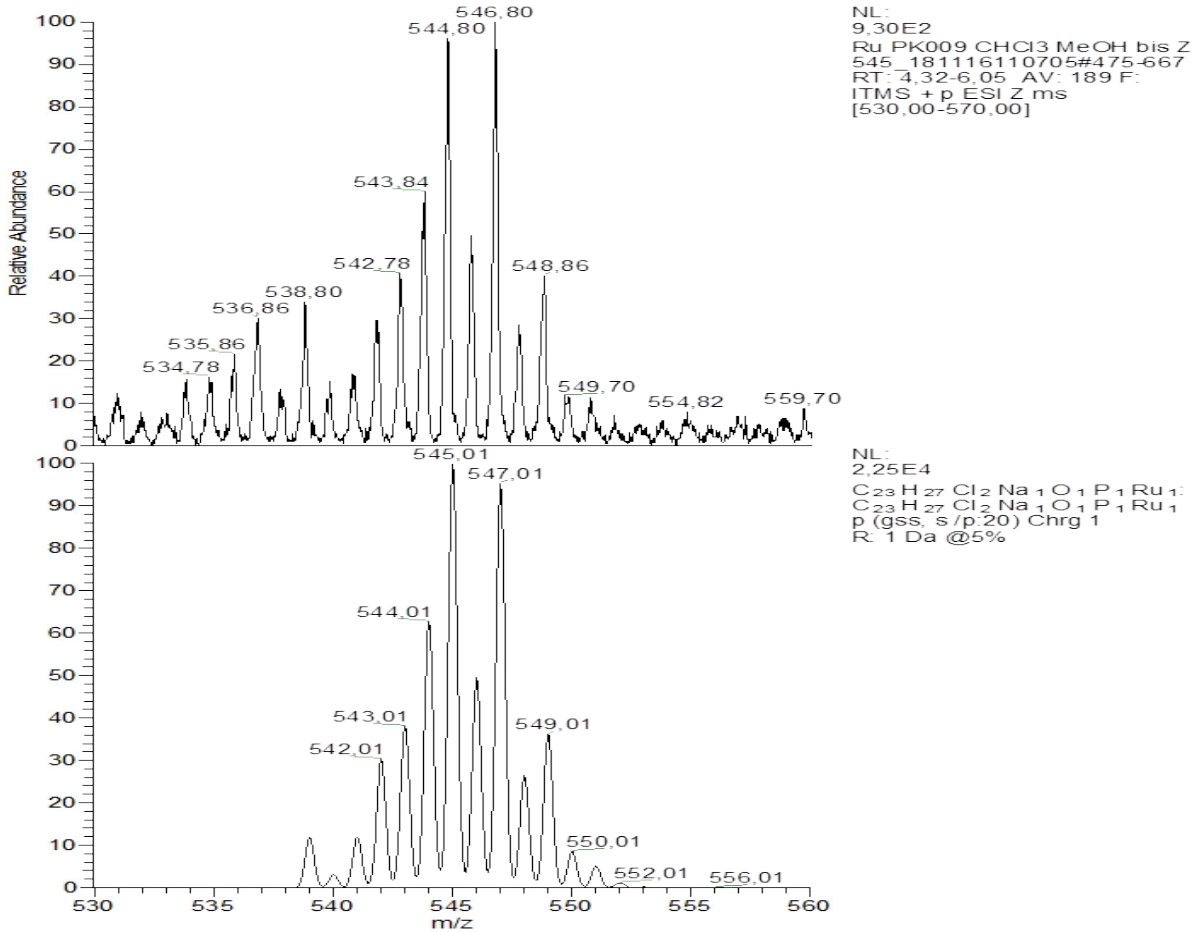

Figure S16. Comparison of the cluster ion peak of **RuPOH** centered at m/z 545 (experimental (top) vs calculated (bottom)) corresponding to the sodiated $[M + Na]^+$ ion.

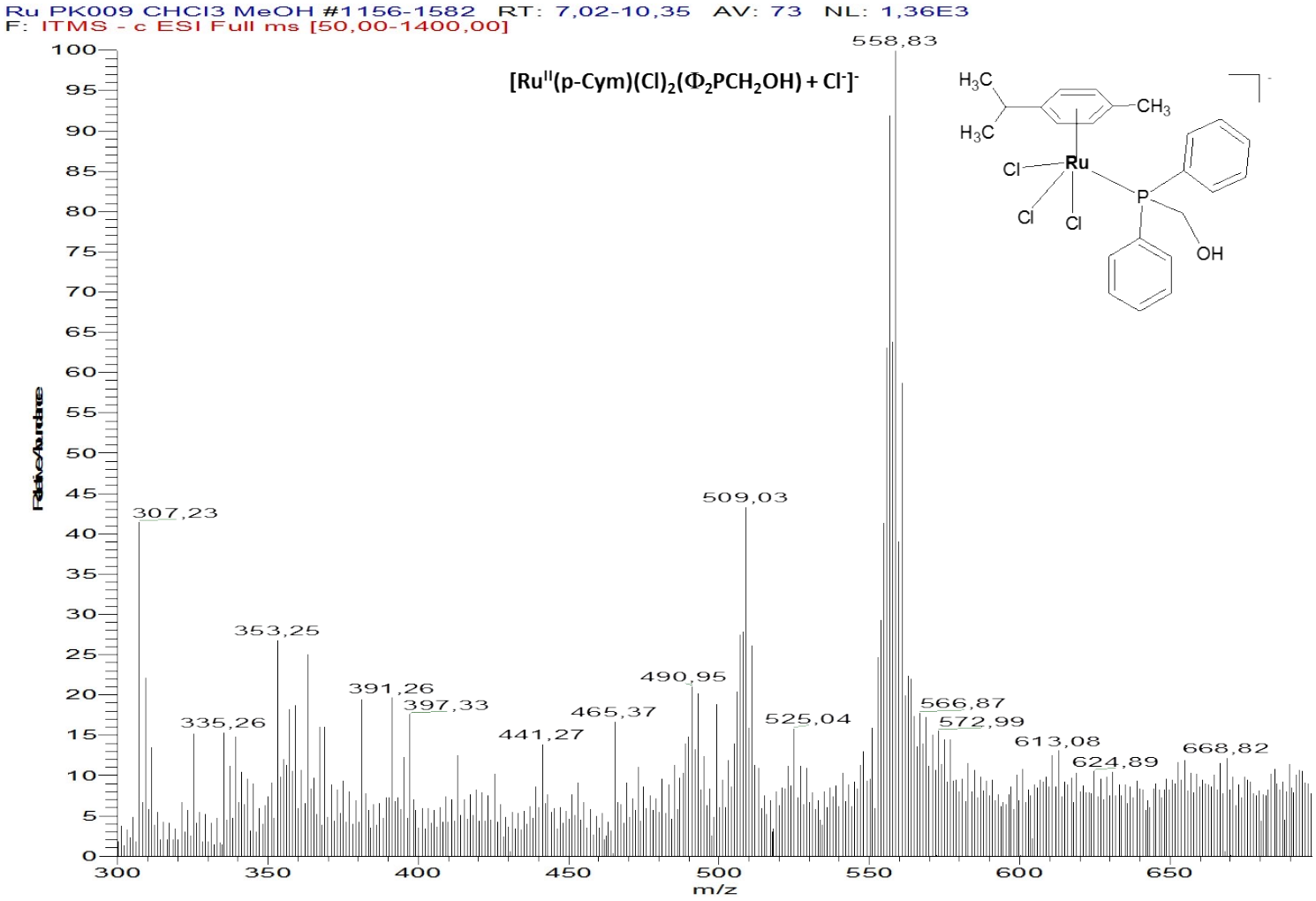

Figure S17. Full ESI(+)MS spectrum of **RuPOH**.

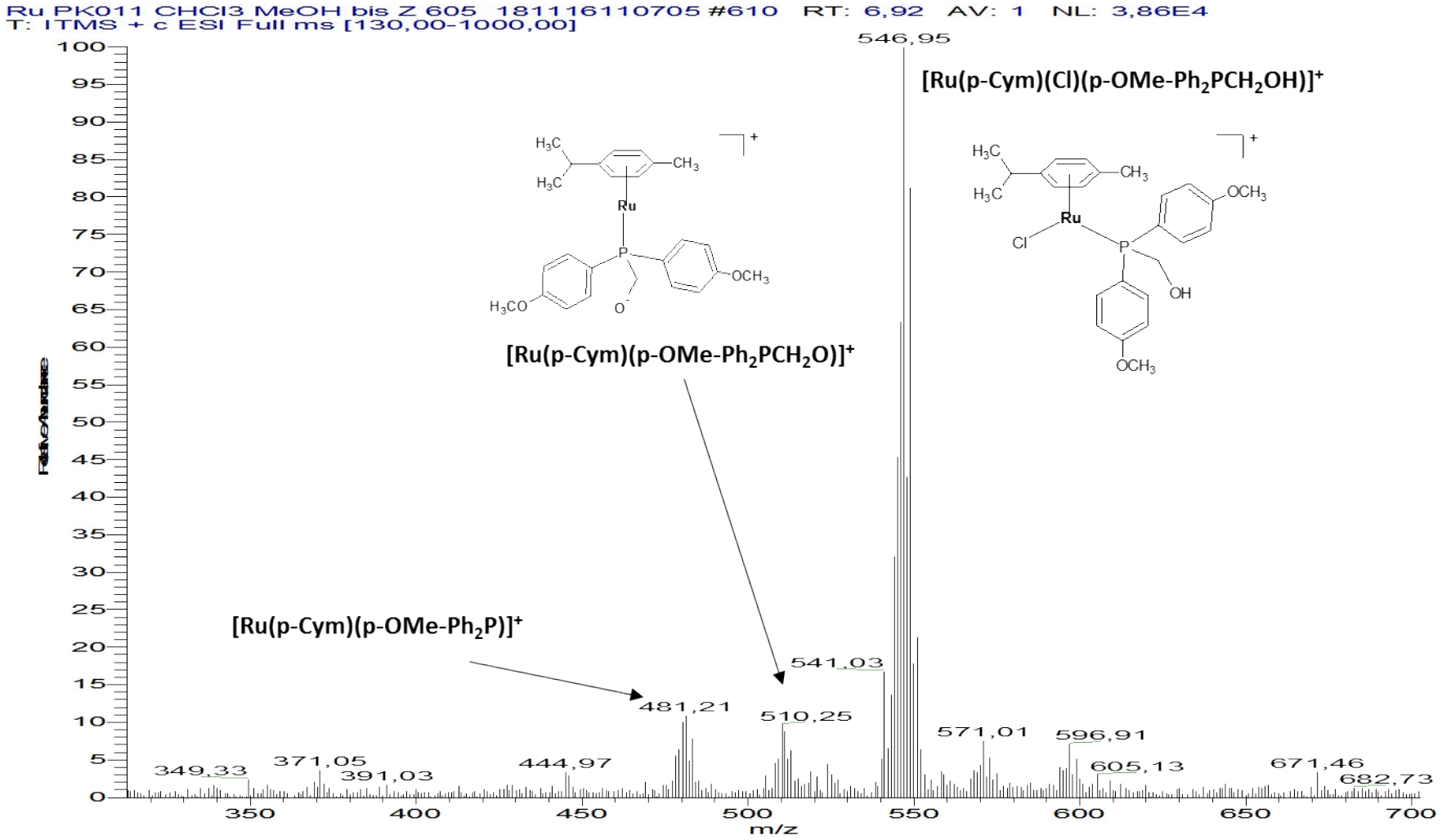

Figure S18. Full ESI(-)MS spectrum of **RuMPOH**.

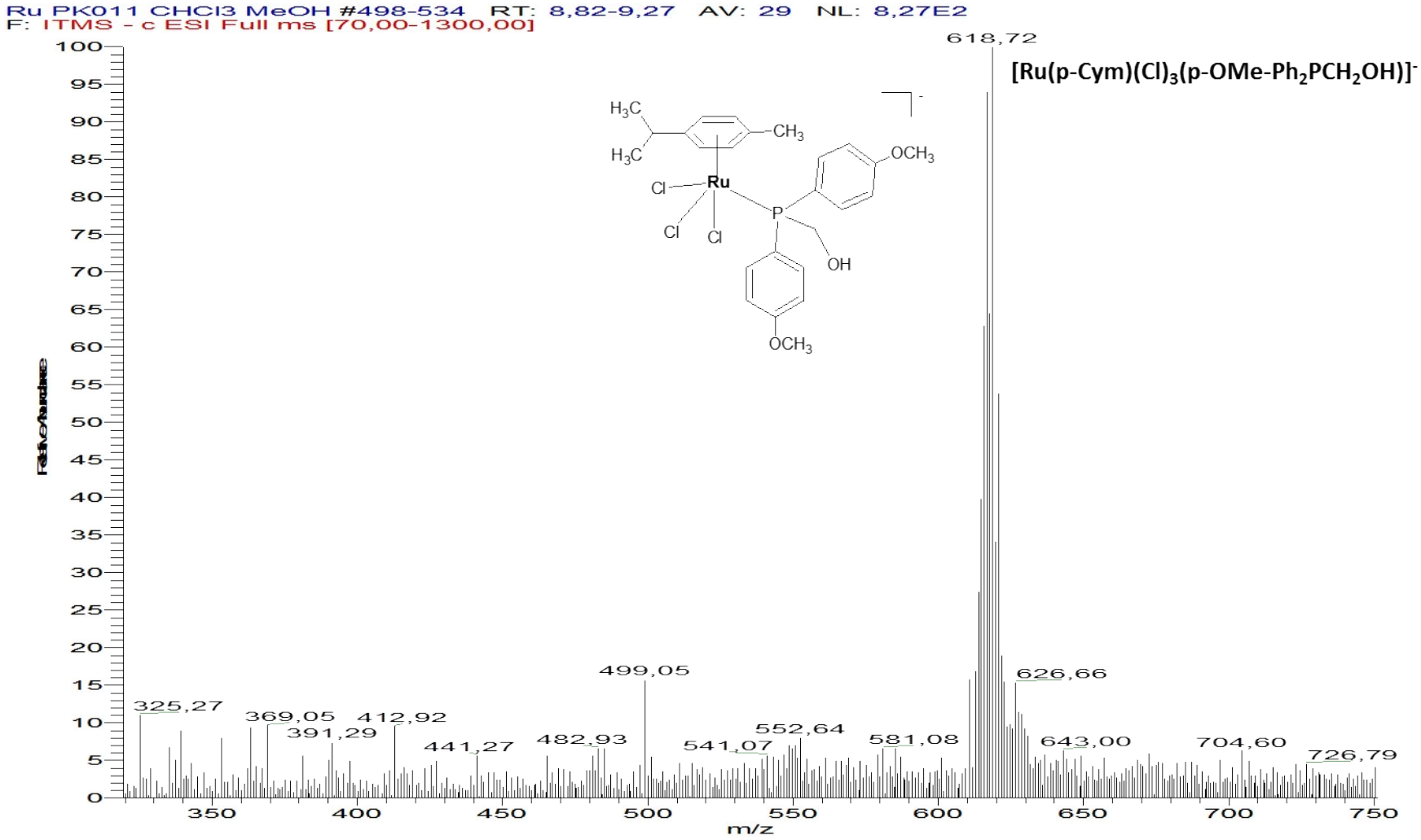

Figure S19. Full ESI(-)MS spectrum of **RuMPOH**.

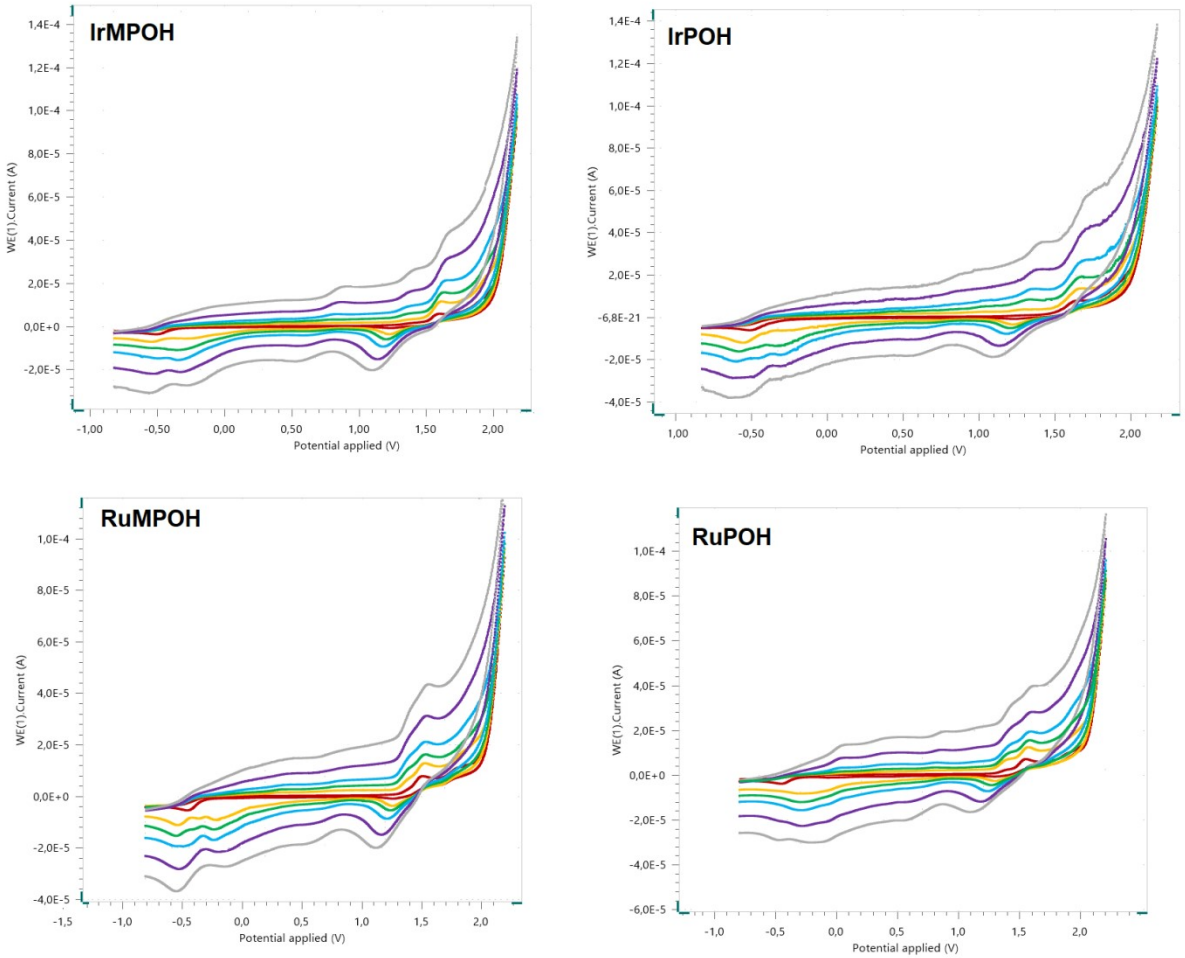

Figure S20. Cyclic voltammetric trace of **RuPOH**, **RuMPOH**, **IrPOH** and **IrMPOH** (1 mM) as a function of scan rate, recorded with recorded with 0.1 M tetrabutyl ammonium perchlorate (TBAP) as supporting electrolyte in DMF solution. Scan rates 1 – 100 (mV s-1). Potential (V) versus $Fc^{0/+}$.

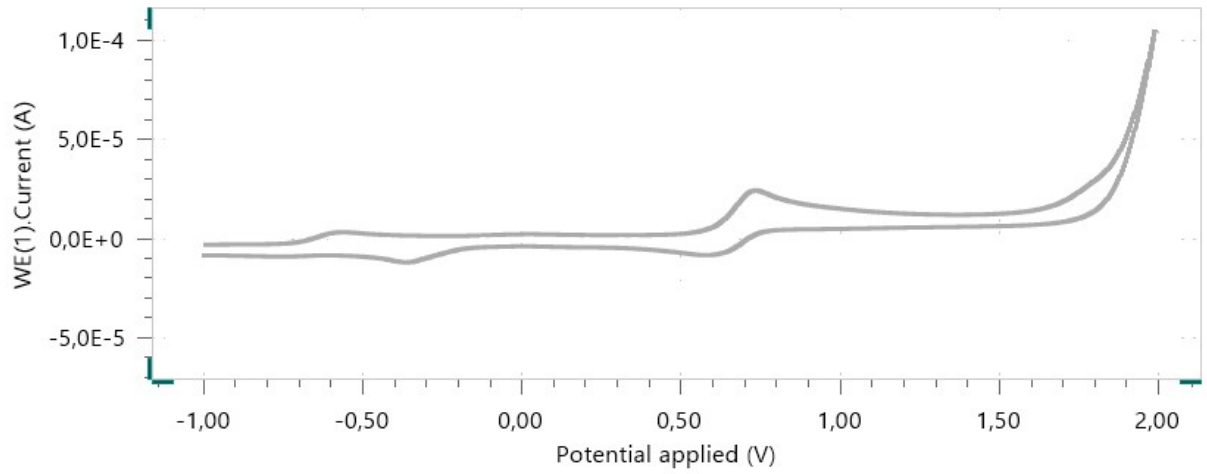

Figure S21. CV voltammograms for ferrocene in DMF in the range of potentials from -01 V to 1.2 V. Scan rate: 10 mV s-1.

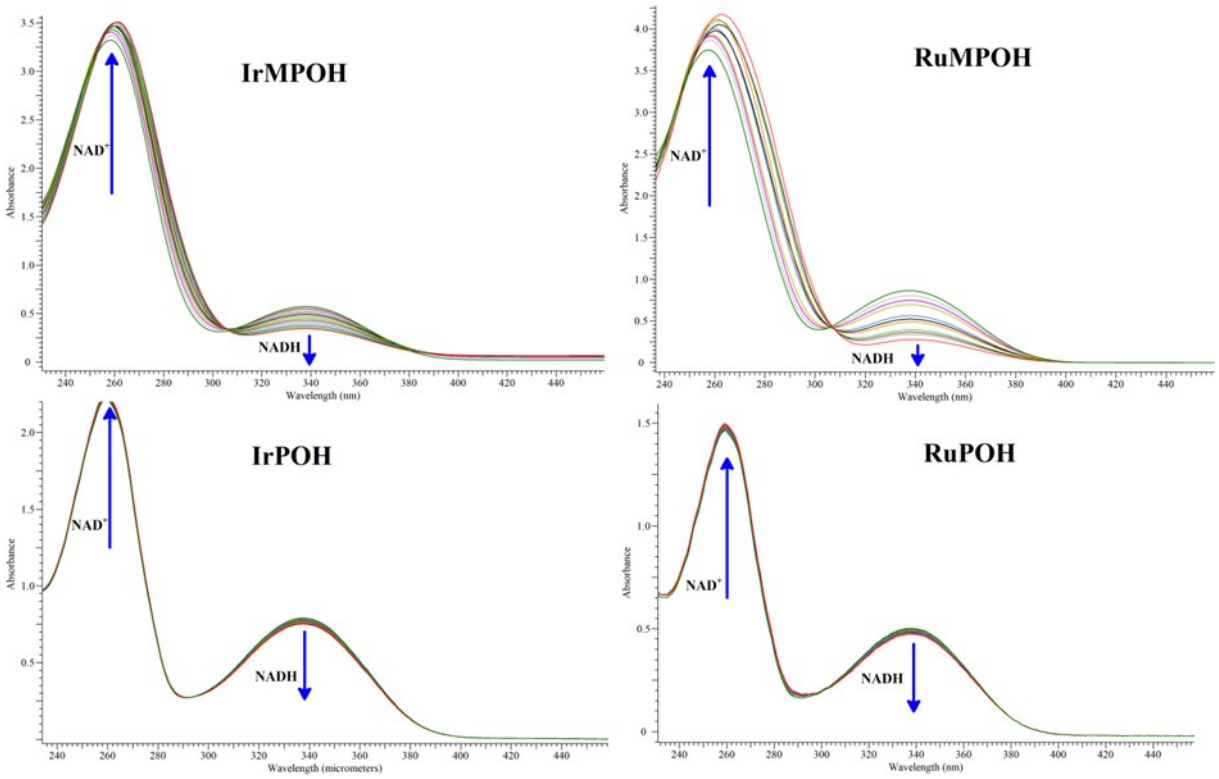

Figure S22. UV/Vis spectra of NADH (100 μM) were determined after incubated with **RuPOH**, **RuMPOH**, **IrPOH**, **IrMPOH** (1 μM) in CH_3OH/H_2O (1 : 9, v/v) at 298 K for 8 h. The arrows show the absorbance change over time.